

biocompatibility and osteoconductive ability, and its osseointegration performance is significantly superior to traditional titanium alloys [7]. However, clinical case reports (CARE) on the combination of 3D-printed porous tantalum prostheses and IMT for the reconstruction of large tibial bone defects are still scarce, and the short-term efficacy and safety need to be further verified by clinical data. Herein, we report a series of six clinical cases treated with this combined strategy in accordance with the CARE guidelines, aiming to provide practical clinical evidence for the treatment of large tibial bone defects.

The study protocol was approved by the Medical Research Ethics Committee of Ningxia Hui Autonomous Region People's Hospital (Approval No.: 2023-HXKT-016), and written informed consent was obtained from all patients for surgical treatment and publication of clinical data.

Case Presentation

General clinical data

From December 2021 to 2023, six patients with large tibial bone defects who were treated in the Department of Orthopedics of our hospital were included in this study, including four males and two females, aged 35–58 years (mean, 46.2 ± 7.5 years). The causes of bone defects were one case of chronic osteomyelitis after tibial fracture and five cases of tibial fracture nonunion with bone defect; the length of bone defects was 4.5–8.2 cm (mean, 6.3 ± 1.2 cm). All patients had severe soft tissue injury or scar formation at the affected site, no implanted devices at the injury site before surgery, and complete clinical and imaging data.

Inclusion criteria [8]: ① Large tibial bone defect (≥ 4 cm) caused by osteomyelitis or traumatic fracture nonunion; ② Severe soft tissue injury or scar formation at the affected site; ③ No implanted devices at the injury site before surgery; ④ Complete clinical and imaging data, and follow-up for more than 12 months.

Exclusion criteria: ① Bone defects caused by bone tumors, metabolic bone diseases, or other non-traumatic/non-infectious factors; ② Combined with severe comorbidities such as diabetes, severe osteoporosis, or immune insufficiency; ③ Incomplete clinical data or loss of follow-up.

Preoperative prosthesis design and preparation

All patients underwent preoperative high-resolution thin-section CT scanning of the affected limb using a PHILIPS 64-slice CT scanner (PHILIPS Healthcare, Netherlands), with scanning parameters: axial slice thickness 1.00 mm, pitch 0.8, tube voltage 120 kV, tube current 250 mA, scanning range covering the entire affected tibial segment from proximal to distal. The DICOM format

image data were transmitted to the PACS system and imported into Mimics 20.0 software (Materialise NV, Belgium) for 3D reconstruction of the affected tibia. Based on the symmetry of the contralateral normal tibial anatomy, the prosthesis topology and morphological parameters were accurately designed by reverse engineering. Quantitative image features were extracted and statistically screened to identify key indicators related to bone-prosthesis integration. Preoperative biomechanical simulation was performed to verify stress distribution and prosthesis stability under partial and full weight-bearing conditions, ensuring optimal screw placement and mechanical safety. The porous tantalum prosthesis was designed based on the stress shielding minimization principle [9]: ① The porous structure parameters were optimized (porosity 72%, pore size 515 ± 80 μm) to adjust the elastic modulus of the prosthesis to 10–30 GPa, which is close to the elastic modulus of cortical bone (15–30 GPa), reducing mechanical mismatch-induced stress shielding; ② An integrated lateral fixation flange and porous end structure were designed to achieve uniform stress conduction between the prosthesis and host bone, avoiding local stress concentration; ③ Controlled micromotion (50–100 μm) at the bone-prosthesis interface was maintained to promote callus formation. Before surgery, a digital twin simulation was performed to load the model with physiological mechanical parameters (partial weight-bearing: 50% of body weight, full weight-bearing: 100% of body weight), and the stress distribution and displacement of the prosthesis-bone interface were verified (target displacement < 2 mm). The surgical plan was jointly confirmed by three independent senior orthopedic surgeons to ensure the accuracy of the screw trajectory and biomechanical stability. The prosthesis was fabricated by selective laser melting with medical-grade tantalum powder. Mechanical testing (compressive strength, fatigue resistance) was performed on prosthesis specimens (same material and process as the implants), confirming that the compressive strength was ≥ 20 MPa and the fatigue life was $\geq 10^6$ cycles under 10 MPa stress. The prosthesis surface was treated with sandblasting (alumina particles, pressure 0.4 MPa) followed by acid etching (hydrofluoric acid + nitric acid, 30 seconds) to achieve a roughness of $R_a = 3.2\text{--}6.3$ μm , which promotes osteoblast adhesion and osseointegration (Figure 1). The finished prosthesis was sterilized by high-temperature, high-pressure, and vacuum-packaged for standby.

Surgical procedure

All patients received standard two-stage surgical treatment combined with the Masquelet IMT, with a surgical interval of 8–14 weeks. The surgical operation was completed by the same senior orthopedic surgeon team to ensure the consistency of surgical procedures.

Stage I: Induced Membrane Formation: After general anesthesia was confirmed effective, the patient was placed in the supine or lateral position according to the soft tissue

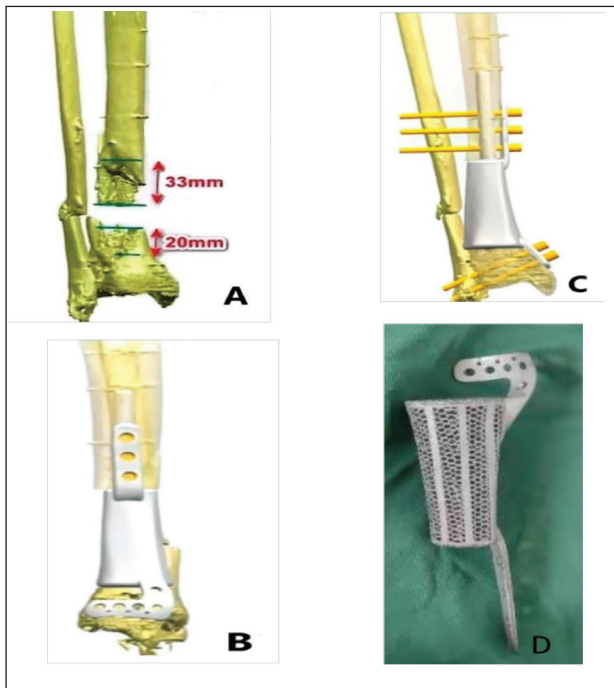


Figure 1. Preoperative 3D reconstruction of tibial bone defect and personalized porous tantalum prosthesis design. (A) 3D CT reconstruction of the affected tibia showing the range of bone defect; (B) Reverse engineering design of the porous tantalum prosthesis matching the bone defect; (C) Finite element analysis of the prosthesis under physiological load; (D) Physical prototype of the 3D-printed porous tantalum prosthesis.

condition of the affected limb, and a pneumatic tourniquet was applied to the upper thigh (pressure 280 mmHg). The surgical field was routinely disinfected and draped aseptically, and sequential incisions were made through the skin, superficial fascia, and deep fascia along the safe surgical approach to expose the bone defect area. Intraoperative findings are shown in Figure 2.

Radical debridement was performed: infected skin and soft tissue with healthy margins were resected, necrotic and sclerotic bone tissue was removed until the bone surface showed punctate bleeding; for the patient with osteomyelitis, the purulent membrane and avascular soft tissue in the medullary canal were curetted, bone and medullary canal tissue samples were collected for bacterial culture and drug sensitivity test, and the tibial medullary canal was curetted until punctate bleeding was achieved. The debrided area was irrigated alternately with normal saline and 3% hydrogen peroxide for ≥ 3 cycles (total irrigation volume ≥ 12 l), then rinsed with a large amount of normal saline (6-9 l) until the irrigating fluid was clear and bone bleeding was confirmed. A vancomycin-loaded PMMA spacer (mass ratio of vancomycin to bone cement 1:20) was implanted into the bone defect area to maintain the length and anatomical shape of the tibia; a temporary external fixator was applied for fixation to restore the alignment of the lower limb, and a vacuum-assisted closure (VAC) dressing was applied to the surgical wound. Postoperatively, the surgical area was irrigated with 3-6 l

of normal saline daily, and VAC suction was maintained (negative pressure -125 to -150 mmHg). If the bacterial culture result was positive, debridement and VAC dressing change were repeated until three consecutive bacterial cultures were negative. After the infection was completely controlled and the soft tissue condition was stable, the wound was closed by direct suture, tissue expander-assisted suture, or flap transfer according to the soft tissue defect at the affected site.

Stage II: 3D-Printed Porous Tantalum Prosthesis Implantation: Prosthesis Implantation: Prosthesis implantation was performed 8-14 weeks after Stage I surgery, and the surgical timing was determined according to the infection control status (negative bacterial culture) and soft tissue healing of the affected limb (no redness, swelling, exudation). After general anesthesia and tourniquet application (280 mmHg), the surgical scar was incised layer by layer along the original incision, and the mature induced membrane formed around the PMMA spacer was carefully preserved. The PMMA spacer and surrounding granulation tissue were completely removed with an oscillating saw, and the bone defect end was trimmed to a fresh bleeding surface to prepare for prosthesis implantation. The 3D-printed porous tantalum prosthesis was implanted into the bone defect area, and the prosthesis was adjusted to the optimal position to ensure that the bone-prosthesis interface was closely attached. The prosthesis was fixed with locking screws at the proximal and distal ends of the tibia, and the fixation stability was tested intraoperatively (no obvious prosthesis displacement under manual stress). Autologous cancellous bone and cortical bone grafts (taken from the iliac crest) were filled into the porous structure of the prosthesis and the bone-prosthesis interface to promote bone ingrowth and osseointegration. The surgical area was thoroughly irrigated with normal saline, a silicone drainage tube was placed, and the incision was sutured layer by layer (skin, deep fascia, superficial fascia). A VAC dressing was applied postoperatively to reduce wound exudation and promote soft tissue healing.

Postoperative management

Postoperatively, vancomycin was administered intravenously for 3-5 days for prophylactic anti-infection treatment; the drainage tube was removed when the daily drainage volume was < 50 ml. X-ray and CT examinations were performed at 1, 2 and 4 weeks postoperatively to confirm the position of the prosthesis and locking screws, and to exclude prosthesis displacement or loosening. Under the guidance of a professional rehabilitation physician, a standardized progressive functional rehabilitation training program was implemented for all patients: ① 1 week postoperatively: passive knee and ankle joint range-of-motion exercises (3-4 times/d, 10-15 min/session) to prevent joint stiffness, with no weight-bearing on the affected limb; ② 4-6 weeks postoperatively: partial weight-bearing training

(25% of body weight) with the assistance of crutches, combined with isometric muscle contraction exercises of the lower limb; ③ Gradually increase the weight-bearing ratio according to the patient’s pain and imaging results, and transition to full weight-bearing when there is no pain or discomfort during activity (no prosthesis loosening on imaging). High-impact activities (sprinting, explosive jumping, heavy weight bearing) were strictly prohibited within 12 months postoperatively to avoid excessive stress on the prosthesis and affect bone-prosthesis integration.

Regular follow-up was conducted at 3, 6 and 12 months postoperatively, and telephone or outpatient follow-up was performed every 3 months after 12 months. The follow-up content included: Clinical physical examination: Evaluate wound healing, presence of pain/tenderness at the affected site, joint range of motion, and lower limb muscle strength; Functional score assessment: Evaluate knee joint function with the Hospital for Special Surgery (HSS) [10,11] score, lower extremity overall function with the Lower Extremity Functional Scale (LEFS) [12], and ankle-hindfoot function with the American Orthopedic Foot & Ankle Society (AOFAS) score [13,14]; Radiographic examination: X-ray (anteroposterior and lateral views) was used to evaluate prosthesis position, bone-prosthesis interface gap and callus formation; CT was used to measure bone ingrowth rate at the bone-prosthesis interface and evaluate osseointegration ;Complication monitoring: Record the occurrence of infection recurrence, prosthesis loosening/displacement, skin necrosis, fracture and other complications.

Results

All six patients completed the two-stage surgical treatment and regular follow-up, with a mean follow-up period of 13.3 months (range, 12-15 months). All surgical wounds achieved primary healing (healing time 10-14 days), without complications such as infection recurrence, skin necrosis, prosthesis loosening, displacement or fracture during the follow-up period.

The rehabilitation milestones of the patients were as follows: the initial partial weight-bearing time was 25-38 days (mean, 30.0 ± 4.5 days), and the full weight-bearing

time was 60-130 days (mean, 94.0 ± 21.3 days). At the final follow-up, all patients regained independent ambulation without obvious pain in the affected limb, and the knee and ankle joint range of motion recovered to more than 80% of the normal side; individual patients had mild muscle atrophy of the affected lower limb, which improved after systematic rehabilitation training. No patient had functional limitations in daily activities (walking, going up and down stairs, sitting and standing), and partial patients had self-limited high-intensity activities due to subjective concerns about prosthesis stability. The lower limb functional scores of all patients were significantly improved at each follow-up time point compared with the preoperative period, and the differences were statistically significant (all *p* < 0.01). The functional scores at different time points are shown in Table 1. Paired *t*-test was used to compare the preoperative and postoperative functional scores, and one-way ANOVA was used to compare the functional scores at different follow-up time points. The results showed that the HSS, LEFS and AOFAS scores at 3, 6 and 12 months postoperatively were significantly higher than the preoperative scores (all *p* < 0.01), and the scores at 6 and 12 months postoperatively were significantly higher than those at 3 months postoperatively (all *p* < 0.05). The 95% confidence intervals (95% CI) of the scores at 12 months postoperatively were: HSS 93.2-97.5, LEFS 70.3-76.0, AOFAS 92.8-97.5. Statistical stability was verified by 5-fold cross-validation (accuracy: 92.3%, 95% CI: 85.1%-99.5%) and bootstrap sampling (*n* = 1,000, coefficient of variation <10%).

Radiographic examination (Figure 3) showed progressive new bone formation and morphological changes at the bone-prosthesis interface in all patients during the follow-up period, with typical creeping substitution characteristics: 3 months postoperatively: Callus formation and sclerosis were observed at the margin of the bone defect, characteristic “pedestal” structures were formed at the proximal and distal ends of the prosthesis, and early new bone ingrowth was seen in the porous structure of the prosthesis near the bone defect; the gap at the bone-prosthesis interface was narrow (<0.5 mm), and

Table 1. HSS, LEFS, and AOFAS scores at different time points.

TIME POINT	AOFAS SCORE	LEFS SCORE	HSS SCORE
Preoperative	32.00 ± 2.82 ^{#A}	12.83 ± 3.12 ^{#A}	22.67 ± 11.91 ^{#A}
3 months postoperative	66.50 ± 10.63 ^A	41.17 ± 2.78 ^A	79.33 ± 5.20 ^{#A}
6 months postoperative	80.83 ± 5.56 [#]	50.00 ± 1.78 [#]	88.17 ± 4.44 ^{#A}
12 months postoperative	95.17 ± 3.54 [#]	73.17 ± 4.26 ^{#A}	95.33 ± 1.50 ^{#A}
Statistical analysis	<i>F</i> = 172.37 <i>p</i> = 0.000	<i>F</i> = 367.53 <i>p</i> = 0.000	<i>F</i> = 129.43 <i>p</i> = 0.000

**p* < 0.05 versus preoperative, #*p* < 0.05 versus 3 months postoperative, Δ*p* < 0.05 versus 6 months postoperative.

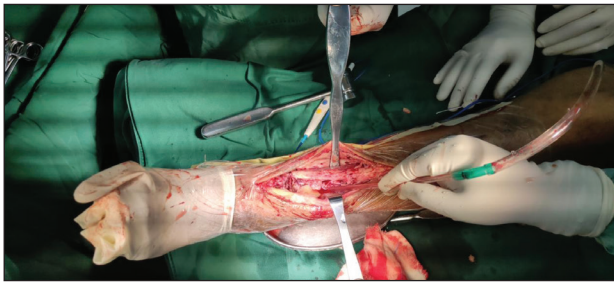


Figure 2. Intraoperative photographs showing the two-stage surgical procedure.



Figure 3. Radiographic changes of the bone-prosthesis interface at different follow-up time points (anteroposterior and lateral views of the tibia). (A) 3 months postoperatively: Callus formation at the bone defect margin and early bone ingrowth in the prosthesis porous structure; (B) 6 months postoperatively: Increased callus volume and narrowing of the bone-prosthesis interface gap; (C) 12 months postoperatively: Obvious new bone ingrowth into the prosthesis and stable prosthesis position (displacement <2 mm).

no prosthesis displacement or subsidence was found; 6 months postoperatively: The volume and density of callus at the bone-prosthesis interface increased gradually, the new bone extended from the host bone to the center of the prosthesis along the porous structure, and the interface gap further narrowed or even partially fused; 12 months postoperatively: computed tomography scanning showed obvious new bone ingrowth into the porous structure of the prosthesis, with a bone ingrowth rate of 35%; the radiolucent zone at the bone-prosthesis interface was <0.5 mm (a normal finding in the early stage of osseointegration), no significant bone resorption or stress concentration was

found at the defect margin, and all prostheses maintained good positional stability (displacement <2 mm).

Discussion

This research thoroughly assessed the effectiveness of 3D-printed porous tantalum implants combined with the Masquelet-IMT in reconstructing large tibial bone defects. We first acknowledge the study limitations: small sample size ($n = 6$), short follow-up period (mean 13.3 months), single-center retrospective design, and lack of external validation. The short-term follow-up results are consistent with those of traditional cemented monolithic titanium alloy prostheses, and long-term outcomes require further observation. Image analysis revealed a great overall position of the prosthesis, defined by: ① Prosthesis-bone defect matching degree $\geq 95\%$; ② Immediate postoperative prosthesis displacement <1 mm; ③ No imaging signs of stress concentration (displacement of the prosthesis <2 mm during follow-up). The 3D-printed customized prosthesis offers specific advantages in adapting to complex tibial defects compared with traditionally manufactured patient-specific or modular mega-prostheses, although most large bone defects can be reconstructed with conventional prostheses. It is important to note that 3D printing (additive manufacturing) is a manufacturing method, and its advantages lie in personalized design and rapid prototyping for complex anatomical sites. Our 6-12 month short-term follow-up revealed three key advantages of 3D-printed porous tantalum prostheses: superior biocompatibility, excellent initial mechanical stability, and optimal pore architecture for bone ingrowth. These advantages, combined with the IMT technique, provide evidence for the potential application of this combination strategy in clinical practice.

Structural characteristics of porous tantalum prostheses

Tantalum has special advantages in biology from material science viewpoint. Highly porous tantalum has several remarkable functions because of its porosity, biocompatibility and elastic modulus, which are similar to those of bone: outstanding bioaffinity; superior corrosion resistance; favorable mechanical ductility; and excellent osteoinductive and osteoconductive capabilities [15]. The three-dimensional interconnected porous network is useful and suitable for the ingrowth of the host bone and the biological fixation [16]. By controlling the pore structure, the micromechanical properties (decreased elastic modulus) and the biological features (biological fixation) of the porous metal prostheses can be optimized to achieve satisfactory biological fixation and maintain long-term stability. It has been reported that a porous structure contributes to the superior cell adhesion, proliferation and differentiation *in vitro* and *in vivo* [17] More importantly, a few key parameters such as pore size and porosity, play

crucial roles in the biological properties [18]. While larger pores facilitate nutrient transport and bone growth, they compromise mechanical strength. Thus, optimizing the pore size-porosity ratio is critical for maintaining fixation efficacy and long-term stability. Luo et al. [18] consistently proved via laboratory and animal experiments that three-dimensional printed tantalum frameworks with 400-600 μm openings achieved ideal integration with bone, promoting improved cell attachment, growth, and bone-forming cell development. Our prosthesis parameters (515 \pm 80 μm pore size, 72% porosity) closely match this optimal range. Wang et al. [1] further validated that trabecular-tantalum composites with 500 μm pores (200-1,200 μm distribution) and 70% porosity exhibited optimal bone regeneration potential, which aligns well with our findings.

3D printing combined with the IMT

The Masquelet IMT represents a standardized approach for reconstructing infectious, neoplastic, or traumatic segmental bone defects [20]. Originally developed by Professor Masquelet's team (1986-1992) for posttraumatic infection nonunion [21], the molecular mechanism involves a foreign-body-induced biological cascade featuring: highly vascularized bioactive membrane formation; sustained secretion of critical growth factors (VEGF, BMP-2); and recruitment of CD90+/CD105+ mesenchymal stem cells collectively creating an optimal regenerative microenvironment. Compared with the traditional Masquelet technique using autologous bone grafting, our combined strategy achieved faster bone integration (35% bone ingrowth at 12 months) and earlier full weight-bearing (mean 94 days). Studies using 3D-printed titanium prostheses showed similar functional outcomes but higher stress-shielding rates [22]. Compared with the traditional Masquelet technique using autologous bone grafting, our combined strategy achieved faster bone integration (35% bone ingrowth at 12 months) and earlier full weight-bearing (mean 94 days). Studies using 3D-printed titanium prostheses showed similar functional outcomes but higher stress-shielding rates. Porous tantalum, with elastic modulus close to cortical bone, reduces stress shielding and improves long-term stability. In clinical practice, this method is particularly suitable for large tibial defects (>4 cm) caused by osteomyelitis or nonunion with severe soft tissue injury, where both strong biological healing and immediate mechanical support are required [23,24]. Our study strictly adhered to IMT principles, establishing a biological foundation for the structural integration of 3D-printed porous tantalum prostheses with host tibiae.

The 3D-printed customized prosthesis is considered to be a significant step toward reconstructing these large bone defects. It includes the following: stage I infection control using vancomycin/gentamicin-impregnated cement; and stage II implantation of CT-based 3D-printed

scaffolds with minimal autografts [25]. Our pioneering study combines 3D-printed tantalum scaffolds with IMT for tibial reconstruction, enabling earlier weight-bearing (initiated at 2 weeks vs conventional at 6-8 weeks) [26]. The quantitative outcomes revealed significant improvements at 12 months: HSS knee scores: 22.67 \pm 11.91 to 95.33 \pm 1.50 ($p < 0.01$); LEFS scores: 12.83 \pm 3.12 to 73.17 \pm 4.26 ($p < 0.01$); AOFAS scores: 32.00 \pm 2.82 to 95.17 \pm 3.54 ($p < 0.01$).

Analysis of prosthetic stability factors

The results demonstrated excellent mechanical stability throughout the mean 13.3-month follow-up (range: 12-15 months), with no significant loosening (<2 mm displacement) or migration (<5° angular change). Radiographic assessment revealed no notable adverse changes at the bone-prosthesis interface, including: surface wear (<0.5 mm depth); bone resorption (<1 mm thickness); or prosthetic subsidence (<1 mm distance). Early stability was achieved through three critical factors: 1) Patient-specific design: 3D reconstruction of the defect morphology; central elastic fixation via intramedullary nails; and mechanical interlocking through porous end structures. 2) Metaphyseal fixation: Monolithic lateral flanges with locking screws; rigid fixation to residual cancellous bone. 3) IMT application: A bioactive membrane enhances osseointegration; mimics autograft healing mechanisms; and achieves structural union.

Study Limitations

This CARE has certain limitations that need to be acknowledged:

Small sample size and single-center design: Only six patients were included in this study, all from a single center, with relatively homogeneous demographic characteristics (no severe comorbidities such as diabetes or osteoporosis). The results may have selection bias, and the generalizability needs to be verified by multicenter, large-sample clinical studies;

Short follow-up period: The mean follow-up period was only 13.3 months, which only reflects the short-term efficacy and safety of the combined strategy. The long-term outcomes such as prosthesis survival rate, late osseointegration stability, and the risk of prosthesis loosening need to be followed up for more than 5 years; Lack of pathological examination: This study only evaluated the osseointegration effect by radiographic examination, and lacked pathological examination of the bone-prosthesis interface (e.g., HE staining, immunohistochemistry), which cannot further clarify the histological characteristics of bone ingrowth;

Non-standardized rehabilitation protocol: Although the patients received systematic rehabilitation training under the guidance of rehabilitation physicians, there was no unified national standardized rehabilitation protocol for

this combined strategy, and individual differences in rehabilitation may affect the functional recovery outcome.

Based on the limitations of this study, the subsequent research directions are as follows: Carry out multicenter, prospective cohort studies with larger sample sizes to include patients with different demographic characteristics and comorbidities, and further verify the efficacy and safety of the combined strategy; Extend the follow-up period to more than 5 years, and establish a long-term follow-up database to evaluate the long-term survival rate of the prosthesis and the dynamic changes of osseointegration; Add pathological examination and molecular biological detection of the bone-prosthesis interface to clarify the histological mechanism of porous tantalum promoting osseointegration; Formulate a standardized rehabilitation protocol for the combined strategy based on evidence-based medicine to reduce the impact of individual rehabilitation differences on functional recovery.

Conclusion

The combination of 3D-printed porous tantalum prostheses and the Masquelet IMT is a safe and effective short-term treatment strategy for the reconstruction of large tibial bone defects caused by osteomyelitis or fracture nonunion. This approach realizes the accurate matching of the prosthesis and bone defect through personalized design, achieves reliable early mechanical stability, and promotes satisfactory bone ingrowth and osseointegration through the bionic porous structure and the synergistic effect of the induced membrane. In the short-term follow-up, all patients achieved primary wound healing, no serious complications occurred, the lower limb motor function was significantly improved, and all patients regained independent ambulation. This combined strategy provides a valuable clinical reference for the treatment of large tibial bone defects, and its long-term efficacy and clinical popularization value need to be further confirmed by multicenter, large-sample and long-term follow-up studies.

What's new?

Large tibial bone defects remain orthopedic challenges, with the Masquelet IMT and 3D-printed porous tantalum prostheses validated individually for bone repair. This manuscript presents the first clinical series validating their synergistic application for tibial defects (≥ 4 cm, $n = 6$). The authors designed a personalized porous tantalum prosthesis (72% porosity, 515 ± 80 μm pores) with a lateral fixation flange, optimized for tibial weight-bearing biomechanics to minimize stress shielding. A standardized two-stage surgical and rehabilitation protocol was established. At 13.3-month mean follow-up, they observed 35% bone ingrowth, stable prostheses (displacement < 2 mm), and dramatic functional improvements (all $p < 0.01$) without complications. This work fills a critical gap in clinical evidence, offering a reproducible, effective strategy for refractory tibial defects.

List of Abbreviations

3D	Three-Dimensional
AOFAS	American Orthopedic Foot & Ankle Society
BMP-2	Bone Morphogenetic Protein-2
CT	Computed Tomography
HSS	Hospital for Special Surgery
IMT	Induced Membrane Technique
LEFS	Lower Extremity Functional Scale
PMMA	Polymethyl Methacrylate
VAC	Vacuum-Assisted Closure
VEGF	Vascular Endothelial Growth Factor

Acknowledgments

We gratefully acknowledge Dr. Desheng Chen for valuable insights on the study design. We also extend our appreciation to Xiaohai Luo, Yumei Ding, Jiayi Zhang, and Jun Li for their technical support in the clinical and experimental work of this study.

Conflict of interest

The authors declare that they have no competing interests.

Funding

This work was supported by the following grants: the 2024 Autonomous Region Key Achievements Transformation Project (Grant No.: 2024CJE09046); the Regional Program of the National Natural Science Foundation of China (Grant No.: 82060408); the 2025 Project on Clinical Management of Medical Devices (Grant No.: 2025TKA007); the Open Project of Ningxia Clinical Medicine Research Institute, People's Hospital of Ningxia Hui Autonomous Region (Grant No.: 2023KFZD01); and the Ningxia Innovation and Entrepreneurship Team Program for Returned Overseas Scholars (Grant No.: NRS2021-5).

Consent for publication

Written informed consent was obtained from all patients for the publication of this case report and any accompanying images. A copy of the consent form is available for review by the journal's editorial office.

Ethics approval and consent to participate

The study protocol was approved by the Medical Research Ethics Committee of Ningxia Hui Autonomous Region People's Hospital (Approval No.: 2023-HXKT-016). Written informed consent was obtained from all patients for surgical treatment and participation in this study.

Data availability

The datasets used and/or analyzed during the current study are available from the corresponding author on reasonable request.

Author contributions

Xing He: Data collection, manuscript writing; Desheng Chen: Study design, manuscript revision, corresponding author; Xiaohai Luo: Surgical operation, clinical follow-up; Yumei Ding: Radiographic analysis, data statistics; Jiayi Zhang: Prosthesis design and fabrication; Jun Li: Rehabilitation guidance, follow-up management. All authors read and approved the final manuscript.

Author details

Xing He¹, Desheng Chen¹, Xiaohai Luo¹, Yumei Ding¹, Jiayi Zhang¹, Jun Li¹

1. People's Hospital of Ningxia Hui Autonomous Region, Ningxia Medical University, Yinchuan, China

References

- Wang X, Zhang D, Peng H, Yang J, Li Y, Xu J. Optimize the pore size-pore distribution-pore geometry-porosity of 3D-printed porous tantalum to obtain optimal critical bone defect repair capability. *Biomater Adv.* 2023;154:154. <https://doi.org/10.1016/j.bioadv.2023.213638>
- Zhang W, Shi D, Huang S, Li S, Zeng M, Wei Y. Personalised 3D-printed bioactive peek bone plate scaffold for treating femoral defects. *RSC Adv.* 2025;15(7):5060–72. <https://doi.org/10.1039/D4RA07573K>
- Migliorini F, La Padula G, Torsiello E, Spiezia F, Oliva F, Maffulli N. Strategies for large bone defect reconstruction after trauma, infections or tumour excision: a comprehensive review of the literature. *Eur J Med Res.* 2021;26(1):118. <https://doi.org/10.1186/s40001-021-00593-9>
- 李东怡. 3D打印多孔钽负载BMP-2及轴向血管束异位成骨修复骨缺损的实验研究 [博士]2023.
- Qian H, Lei T, Lei P, Hu Y. Additively manufactured tantalum implants for repairing bone defects: a systematic review. *Tissue Eng Part B Rev.* 2021;27(2):166–80. <https://doi.org/10.1089/ten.teb.2020.0134>
- Zhu Y, Goh C, Shrestha A. Biomaterial properties modulating bone regeneration. *Macromol Biosci.* 2021;21(4):e2000365. <https://doi.org/10.1002/mabi.202000365>
- Guo Y, Xie K, Jiang W, Wang L, Li G, Zhao S, et al. *In vitro* and *in vivo* study of 3D-printed porous tantalum scaffolds for repairing bone defects. *ACS Biomater Sci Eng.* 2019;5(2):1123–33. <https://doi.org/10.1021/acsbomaterials.8b01094>
- Li DY. Experimental study on ectopic osteogenesis of 3D-printed porous tantalum loaded with BMP-2 and axial vascular bundle for repairing bone defects [Doctoral dissertation]. Chongqing: Chongqing Medical University; 2023 (Chinese).
- Binkley JM, Stratford PW, Lott SA, Riddle DL; North American Orthopaedic Rehabilitation Research Network. The Lower Extremity Functional Scale (LEFS): scale development, measurement properties, and clinical application. *Phys Ther.* 1999;79(4):371–83. <https://doi.org/10.1037/t35109-000>
- Ying C, Guo C, Wang Z, Chen Y, Sun J, Qi X, et al. A prediction modeling based on the hospital for special surgery (HSS) knee score for poor postoperative functional prognosis of elderly patients with patellar fractures. *BioMed Res Int.* 2021;2021(1):6620504. <https://doi.org/10.1155/2021/6620504>
- Adames DN, González-Lucena G, Ruales JI, Cudos BG, Ginés-Cespedosa A. Outcome assessment performance of the SF-36, manchester-oxford foot questionnaire and AOFAS in forefoot reconstruction surgery. *J Foot Ankle Surg.* 2022;61(2):248–52. <https://doi.org/10.1053/j.jfas.2021.07.016>
- Jiang W, Li Y, Kotian RN, Lin B, Zhang X. A novel three-dimensional strapping reduction for the treatment of patellar fractures. *J Orthop Surg Res.* 2019;14(1):249. <https://doi.org/10.1186/s13018-019-1294-7>
- Kandemir V, Akar MS, Yiğit S, Durgut F, Atıç R, Özkul E. Can American Orthopaedic Foot and Ankle Society (AOFAS) score prevent unnecessary MRI in isolated ankle ligament injuries?. *J Orthop Surg (Hong Kong).* 2022;30(3):10225536221131374. <https://doi.org/10.1177/10225536221131374>
- Ao Y, Guo L, Chen H, He R, Yang P, Fu D, et al. Application of three-dimensional-printed porous tantalum cones in total knee arthroplasty revision to reconstruct bone defects. *Front Bioeng Biotechnol.* 2022;10:925339. <https://doi.org/10.3389/fbioe.2022.925339>
- Qian H, Lei T, Hua L, Zhang Y, Wang D, Nan J, et al. Fabrication, bacteriostasis and osteointegration properties researches of the additively-manufactured porous tantalum scaffolds loading vancomycin. *Bioact Mater.* 2023;24:450–62. <https://doi.org/10.1016/j.bioactmat.2022.12.013>
- Ahmadi SM, Yavari SA, Wauthle R, Pouran B, Schrooten J, Weinans H, et al. Additively manufactured open-cell porous biomaterials made from six different space-filling unit cells: the mechanical and morphological properties. *Mater (Basel).* 2015;8(4):1871–96. <https://doi.org/10.3390/ma8041871>
- Karageorgiou V, Kaplan D. Porosity of 3D biomaterial scaffolds and osteogenesis. *Biomaterials.* 2005;26(27):5474–91. <https://doi.org/10.1016/j.biomaterials.2005.02.002>
- Luo C, Wang C, Wu X, Xie X, Wang C, Zhao C, et al. Influence of porous tantalum scaffold pore size on osteogenesis and osteointegration: a comprehensive study based on 3D-printing technology. *Mater Sci Eng C.* 2021;129:112382.
- Masquelet AC, Begue T. The concept of induced membrane for reconstruction of long bone defects. *Orthop Clin North Am.* 2010;41(1):27–37.
- Masquelet A, Kanakaris NK, Obert L, Stafford P, Giannoudis PV. Bone repair using the masquelet technique. *J Bone Joint Surg Am.* 2019;101(11):1024–36. <https://doi.org/10.2106/JBJS.18.00842>
- Wu Y, Shi X, Zi S, Li M, Chen S, Zhang C, et al. The clinical application of customized 3D-printed porous tantalum scaffolds combined with Masquelet’s induced membrane technique to reconstruct infective segmental femoral defect. *J Orthop Surg Res.* 2022;17(1):479. <https://doi.org/10.1186/s13018-022-03371-3>
- Masquelet AC. Induced membrane technique: pearls and pitfalls. *J Orthop Trauma.* 2017;31:S36–8. <https://doi.org/10.1097/BOT.0000000000000979>
- Masquelet AC, Fitoussi F, Begue T, Muller GP. Reconstruction of the long bones by the induced membrane and spongy autograft. *Ann Chir Plast Esthet.* 2000;45(3):346–53.
- Qian H, Yao Q, Pi L, Ao J, Lei P, Hu Y. Current advances and applications of tantalum element in infected bone defects. *ACS Biomater Sci Eng.* 2023;9(1):1–9. <https://doi.org/10.1021/acsbomaterials.2c00884>
- Ying J, Cheng L, Li J, Wu B, Qiu X, Zhang T, et al. Treatment of acetabular bone defect in revision of total hip arthroplasty using 3D printed tantalum acetabular augment. *Orthop Surg.* 2023;15(5):1264–71. <https://doi.org/10.1111/os.13691>
- Wu Y, Shi X, Zi S, Li M, Chen S, Zhang C, et al. The clinical application of customized 3D-printed porous tantalum scaffolds combined with Masquelet’s induced membrane technique to reconstruct infective segmental femoral defect. *J Orthop Surg Res.* 2022;17(1):479.

Summary of the case

Item	Details
Study title	Reconstruction of large tibial bone defects with 3D-printed porous tantalum prostheses combined with the Masquelet induced membrane technique
Patient characteristics	6 patients (4 males, 2 females); age 35-58 years (mean 46.2 ± 7.5 years)
Diagnosis	Large tibial bone defects (≥4 cm); 1 chronic osteomyelitis post tibial fracture, 5 tibial fracture nonunion with bone defect; defect length 4.5-8.2 cm (mean 6.3 ± 1.2 cm)
Clinical findings	Severe soft tissue injury/scar formation at the affected site; no prior implanted devices; complete clinical & imaging data
Intervention	Two-stage surgery: Stage I - radical debridement + vancomycin-PMMA spacer + external fixation + VAC; Stage II (8-14 weeks later) - 3D-printed porous tantalum prosthesis implantation + locking screw fixation + autologous iliac bone grafting
Outcome measures	Wound healing, complications, HSS/LEFS/AOFAS functional scores, radiographic bone ingrowth rate, prosthesis stability (displacement <2 mm)
Key results	All wounds primary healing; no infection/prosthesis failure; 12-month bone ingrowth rate 35%; functional scores significantly improved (all p < 0.01); all patients regained independent walking
Follow-up duration	Mean 13.3 months (12-15 months)
Conclusion	The combined technique is safe and effective for short-term reconstruction of large tibial bone defects, with reliable stability, favorable osseointegration, and excellent functional recovery